https://doi.org/10.3847/1538-4357/aac204

# Why the Shock-ICME Complex Structure Is Important: Learning from the Early 2017 September CMEs

Chenglong Shen[1,2,3], Mengjiao Xu[1], Yuming Wang[1,4], Yutian Chi[1], and Bingxian Luo[5,6]

[1] CAS Key Laboratory of Geospace Environment, Department of Geophysics and Planetary Sciences, University of Science & Technology of China, Hefei, Anhui 230026, People's Republic of China; clshen@ustc.edu.cn
[2] Synergetic Innovation Center of Quantum Information & Quantum Physics, University of Science and Technology of China, Hefei, Anhui 230026, People's Republic of China
[3] Collaborative Innovation Center of Astronautical Science and Technology, Hefei, 230026, People's Republic of China
[4] Mengcheng National Geophysical Observatory, School of Earth and Space Sciences, University of Science and Technology of China, Hefei, 230026, People's Republic of China
[5] National Space Science Center, Chinese Academy of Sciences, No. 1 Nanertiao Zhongguancun Haidian District, Beijing, 100190, People's Republic of China
[6] School of Astronomy and Space Science University of Chinese Academy of Sciences, Yuquan Road, Shijingshan District, Beijing, 100049, People's Republic of China

## Abstract

In the early days of 2017 September, an exceptionally energetic solar active region AR 12673 aroused great interest in the solar physics community. It produced four X class flares, more than 20 coronal mass ejections (CMEs), and an intense geomagnetic storm, for which the peak value of the Dst index reached up to $-142$ nT at 2017 September 8 02:00 UT. In this work, we check the interplanetary and solar source of this intense geomagnetic storm. We find that this geomagnetic storm was mainly caused by a shock-interplanetary CME (ICME) complex structure, which was formed by a shock driven by the 2017 September 6 CME propagating into a previous ICME, which was the interplanetary counterpart of the 2017 September 4 CME. To better understand the role of this structure, we conduct a quantitative analysis on the enhancement of ICME's geoeffectiveness induced by the shock compression. The analysis shows that the shock compression enhanced the intensity of this geomagnetic storm by a factor of two. Without shock compression, there would have been only a moderate geomagnetic storm with a peak Dst value of $\sim-79$ nT. In addition, the analysis of the proton flux signature inside the shock-ICME complex structure shows that this structure also enhanced the solar energetic particle intensity by a factor of approximately five. These findings illustrate that the shock-ICME complex structure is a very important factor in solar physics study and space weather forecast.

*Key words:* solar–terrestrial relations – Sun: coronal mass ejections (CMEs)

## 1. Introduction

Coronal mass ejections (CMEs) are the most energetic eruptions from the Sun. When CMEs continuously erupt from the Sun, they may interact with each other during the propagation from the Sun to 1 au (e.g., Gopalswamy et al. 2001b). Using the large field view observations from the Heliospheric Imager (HI) on board the *Solar TErrestrial RElations Observatory* (*STEREO*; Kaiser et al. 2008), the kinematic evolution of CMEs have been widely studied (e.g., Lugaz et al. 2012, 2017; Shen et al. 2012a, 2017b; Temmer et al. 2012, 2014; Colaninno & Vourlidas 2015; Manchester et al. 2017; Mishra et al. 2017, and references therein). These results show that the space weather effect of CMEs, such as when and which CME structures will impact the Earth, can be greatly effected during the CME's interaction.

The interaction between multiple CMEs can form complex structures as seen from the in situ measurements. Such complex structures have been called complex ejecta, or multiple interplanetary CMEs (ICMEs; e.g., Burlaga et al. 2002). If the ICMEs show obvious characters of magnetic clouds (MC), they are also referred to multiple MCs (e.g., Wang et al. 2003c). In addition, when the shock driven by the following CME propagates into the previous CME, they may form a special type of complex structure called shock-ICME (or shock-MC) structure (e.g., Ivanov 1982; Lepping et al. 1997; Wang et al. 2003c; Lugaz et al. 2015b; Shen et al. 2017a). In such structures, the shock will compress the

magnetic field inside the ICME, thereby often enhancing the geoeffectiveness of the ICME, according to previous case studies (e.g., Lepping et al. 1997; Wang et al. 2003e; Lugaz et al. 2015a), analytical study (Wang et al. 2003d), magnetohydrodynamic (MHD) simulations (e.g., Vandas et al. 1997; Lugaz et al. 2005; Xiong et al. 2006; Shen et al. 2011, 2012b), and statistical analyses (Lugaz et al. 2015b; Shen et al. 2017a). For the space weather study and forecasting, the most important thing is the enhancement of ICMEs' geoeffectiveness caused by the shock compression. Based on a simple theoretical model, Wang et al. (2003d) studied the possible effect of the shock compression on the geoeffectiveness of the shock-ICME structure, and suggested that one time enhancement of $vB_s$ would enhance the Dst index by 1.73 times based on an empirical formula relating the Dst index to the interplanetary parameters.

In addition, Solar Energy Particle (SEP) events are another important space weather phenomena that may be affected by the interaction between shock and ICME. Shen et al. (2008) reported that the proton flux was significantly enhanced in the shock-MC structure in the 2001 November 5 event, which differed from the normal picture that the proton flux would decrease in isolated ICME structures (e.g., Cane & Lario 2006, and references therein). This enhancement might be due to the combined effects of the shock and the MC boundaries: the shock can accelerate particles within the MC, and the MC boundaries prevent the leakage of these accelerated particles. It

is worth noting that the enhancement in the shock-MC structure in the 2001 November 5 event is associated with the largest SEP event in solar cycle 23.

In the early days of 2017 September, the active region AR 12673 passed across the visible side of the Sun. This extremely energetic active region produced more than 80 flares including four X class flares within 7 days. Two of the four X class flares, X9.3 and X8.2 flares (e.g., Yan et al. 2018a, 2018b), are ranked as the top two flares in solar cycle 24 until now. AR 12673 also produced more than 20 CMEs from 2017 September 4 to 10. Thus, we can expect that these CMEs may interact with others during their propagations from the Sun to the Earth. In addition, an intense geomagnetic storm occurred at 2017 September 8 02:00 UT with a peak Dst value ($Dst_{min}$) of −142 nT according to the real time Dst observation provided by World Data Center (WDC). Based on the in situ observations by the *Wind* and *Deep Space Climate ObseRvatory* (*DSCOVR*) spacecraft near the Earth, an obvious shock-ICME complex structure was the main source of this intense geomagnetic storm. Thus, in the paper, we will mainly focus on the space weather effect of shock-ICME complex structures in this period. The detailed in situ observations of ICMEs and their solar sources will be presented in Section 2. In Section 3, we will quantitatively discuss the significance of the shock-ICME complex structure in generating the geomagnetic storms. The influence of the shock-ICME complex structure on SEP intensity will be investigated in Section 4. We will give the conclusions and make some brief discussions in the last section.

## 2. Interplanetary and Solar Sources of the Geomagnetic Storms

To check the geomagnetic activity and the possible interplanetary drivers of the geomagnetic storm, in situ observations from 2017 September 6 to 11 from the *Wind* (black symbols) and *DSCOVR* (red symbols) spacecraft as well as the Dst observations from WDC are shown in Figure 1. Seen from this figure, there was an intense and multi-step geomagnetic storm. The peak of the storm occurred at 2017 September 8 02:00 UT with a value of −142 nT. The sudden commencement of this storm occurred at 2017 September 7 01:00 UT after the first shock (shown as the first vertical blue line) arrived at the Earth. Soon later, the Dst index began to decrease when the sheath region and the ejecta region (Ejecta-1) of the first ICME (called as ICME-1 hereafter) hit the Earth. The leading edge of Ejecta-1 arrived at the Earth on 2017 September 07 06:50 UT and the trailing edge of it arrived at 2017 September 07 11:30 UT (shown by the first shaded region). During this period, the in situ observations exhibited obvious signatures of an MC with enhanced magnetic field intensity, smooth rotated magnetic field vector, low temperature, and low plasma beta. After the passage of ICME-1, the Dst index began to recover. About 10 hr later, the Dst index started to decrease again when the second ejecta (shown by the second shaded region as Ejecta-2/ICME-2) hit the Earth. The ICME-2 started at 2017 September 07 16:50 and ended at 2017 September 08 01:00 UT. Meanwhile, *Wind* and *DSCOVR* recorded a shock at 2017 September 7 22:28 UT, before the trailing edge of ICME-2. It means that this shock was propagating inside the ejecta region of ICME-2 and formed a shock-ICME complex structure. Seen from panel (j) in Figure 1, the Dst index decreased quickly since the arrival of

the shock inside ICME-2. This sudden and quick decrease owed to the large south component of the magnetic field in the ejecta region of ICME-2, which was compressed by the shock. At 2017 September 8 02:00 UT, the Dst index reached its peak value of −142 nT. Thus, this intense geomagnetic storm was mainly caused by the shock-ICME complex structure. After that, two other ejecta were observed near the Earth. They are marked as the third and fourth shaded regions in Figure 1. The third shaded region (called as Ejecta-3 hereafter) has the signature of enhanced magnetic field, low proton temperature, and bi-direction electron beam. But, no obvious rotation of the magnetic field vector can be found. All of the magnetic field carried by this structure points southward. This structure caused another Dst peak with the value of −124 nT. The fourth shaded region in Figure 1 is a long-lasting ejecta (referred to Ejecta-4 hereafter) from 2017 September 08 19:30 UT to September 11 00:00 UT.

Overall, there are two shocks and four ejectas recorded by the in situ measurements near the Earth from September 6 12:00 UT to September 11. The shock times, begin and end times of these ejectas are shown in rows 2–4 of Table 1. In order to find the possible solar sources of these structures, we further check the coronagraph observations of *STEREO-A* and *SOHO* 2017 September 3–8. Figure 2 shows the relative position of Earth and *STEREO* satellites. During this period, the separation angle between Earth and *STEREO A* is ∼128°. Thus, an Earth-directed CMEs can be well observed by the *STEREO-A*. Figure 3 shows the Time-Elongation Angle map from 2017 September 3 to 8. A 64-pixel wide slice is placed along the ecliptic plane in the running-difference images from COR2, HI1, and HI2 on board *STEREO-A* to produce this J-map. Seen from this figure, three different trajectories, which correspond with three CMEs, can be well observed. Meanwhile, the coronagraph images from *STEREO-A* and *SOHO* also show that there are three Earth-directed CMEs erupted from the Sun during this period. Figure 4 shows the coronagraph images of these CMEs. The first CME (CME-1) was first observed by *STEREO A* at 2017 September 4 18:54 UT and was first observed by *SOHO*/LASCO at 2017 September 4 19:00 UT. The front edge of this CME creates the first track in the J-map shown as the red symbols in Figure 3. About 1 hr later, another Earth-directed CME (CME-2) appeared in the *SOHO* and *STEREO-A* field of view. Panels (c) and (d) show the coronagraph observations of this CME. This CME was first observed by *STEREO A* at 2017 September 4 19:54 UT and was first observed by *SOHO* at 2017 September 4 20:36 UT. Seen from *SOHO*, this is a halo CME. The second trajectory in Figure 3, which is indicated by blue symbols, shows the position of the front edge of this CME. Another Earth-directed CME (CME-3) was observed by *SOHO* and *STEREO-A* about two days later. At 2017 September 6 11:54 UT, this CME was first observed by *STEREO-A*/COR2 at its south west direction. Half an hour later, this CME was observed by *SOHO*/LASCO at 2017 September 6 12:24 UT. This CME was associated with a X9.2 class flare and appeared a halo CME in the *SOHO*/LASCO observations. Green symbols in Figure 3 show the position of its front edge and panels (e) and (f) show the coronagraph images of this CME. The fifth column in Table 1 shows the time when these CMEs were first observed by *SOHO*/LASCO.

In addition, the graduated cylindrical shell (GCS) model, which was developed by Thernisien et al. (2006, 2009) and
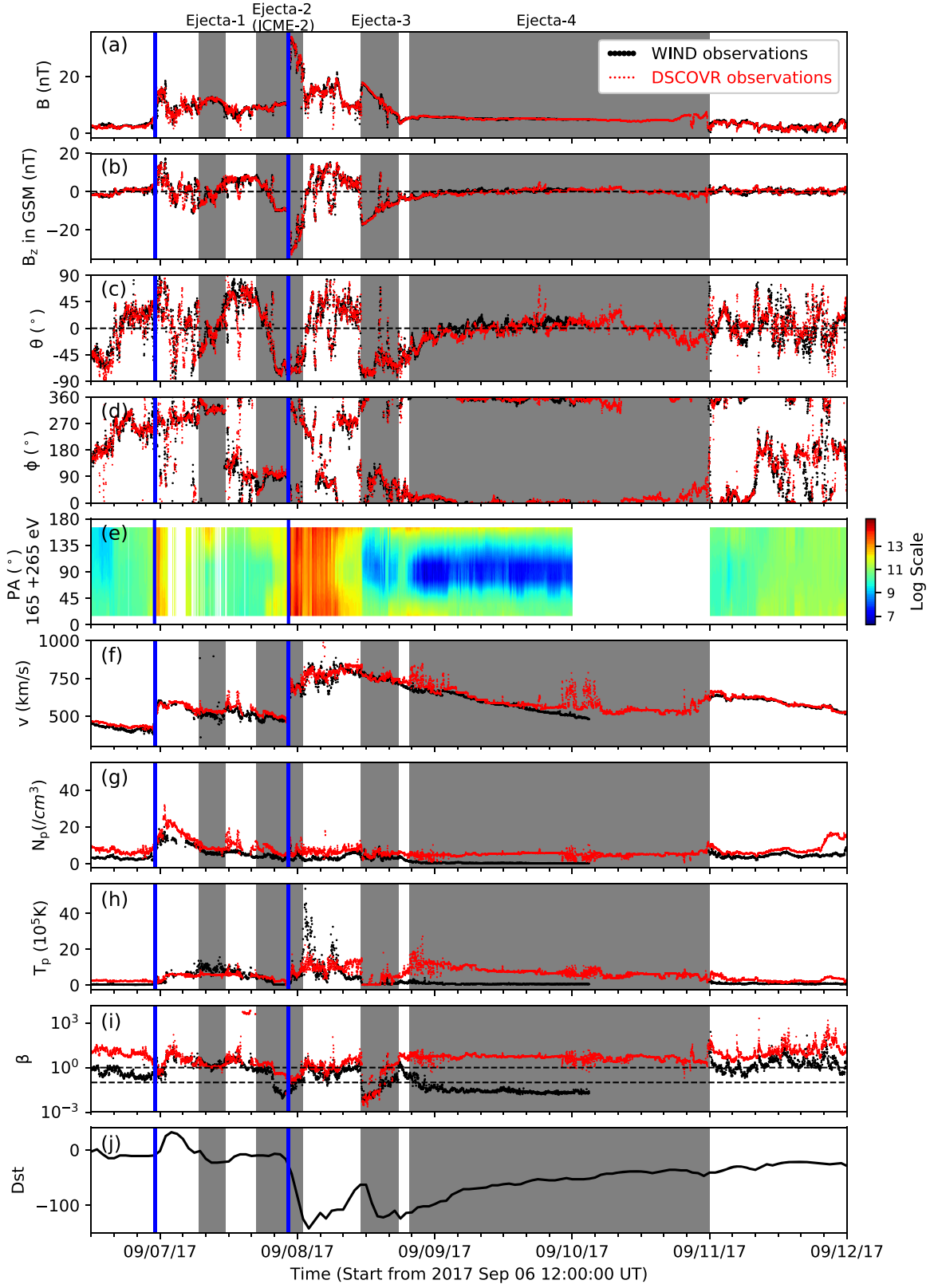
**Figure 1.** The *Wind* and *DSCOVR* in situ observations from 2017 September 6 to 13. The black symbols show the *WIND* observations while the red symbols show the *DSCOVR* observations. From top to bottom, panels are the magnetic field strength ($B$), north component of the magnetic field in GSM coordinate system ($B_z$), the elevation ($\theta$) and azimuthal ($\phi$) of magnetic field direction in GSM coordinate system, solar wind speed ($v$), proton density ($N_p$), proton temperature ($T_p$), the ratio of proton thermal pressure to magnetic pressure ($\beta$), and the Dst from World Data Center (WDC). Shade regions show the period of the ICMEs while the blue vertical lines show the time of shocks.

THE ASTROPHYSICAL JOURNAL, 861:28 (9pp), 2018 July 1                                                                    Shen et al.

**Table 1**
The List of the ICMEs or ICME-like Structures and Their Solar Sources from 2017 September 6 to 9

| No | Shock Arrival (UT) | Begin (UT) | End (UT) | CME Time (UT)[a] | Propagation Direction | Velocity (km s$^{-1}$) | Face-on Width (°) |
|---|---|---|---|---|---|---|---|
| 1 | Sep 6 23:06 | Sep 7 06:50 | Sep 7 11:30 | Sep 4 19:00 | S08W25 | 1005 | 73 |
| 2 | ⋯ | Sep 7 16:50 | Sep 8 01:00 | Sep 4 20:24 | S25W03 | 1766 | 75 |
| 3 | ⋯ | Sep 8 11:05 | Sep 8 17:38 | | | | |
| 4 | Sep 7 22:28 | Sep 8 19:30 | Sep 11 00:00 | Sep 6 12:24 | S18W14 | 1548 | 80 |

**Note.**
[a] The time of this CME was first observed by *SOHO*/LASCO.



**Figure 2.** Positions of *STEREO A*, Earth, and *STEREO B* at the time of 2017 September 5. Different color arrows show the propagation directions of different CMEs.

Thernisien (2011), is applied to obtain the three-dimensional parameters of these CMEs. Figure 5 shows the fitting results of these CMEs. Seen from these images, the GCS model can well represent the topology of these CMEs. The last three columns in Table 1 show the fitting results of these CMEs, including the propagation directions, velocities and face-on angular widths. Assuming a constant velocity and considering the influence of the propagation direction and angular width on the prediction of the arrival time suggested by Shen et al. (2014), CME-1 would arrive at the Earth around the time of September 6 22:27 UT. However, previous results show that fast CME would decelerate during their propagation in interplanetary space (e.g., Gopalswamy et al. 2001a, 2005; Vršnak 2001; Vršnak & Žic 2007; Temmer et al. 2011; Lugaz & Kintner 2012, and reference therein). Such deceleration may make the CME-1 arrive at the Earth later than September 6 22:27 UT. Thus, CME-1 is more likely to be the solar source of ICME-1. Seen from the Figure 3, the front edge of the CME-2 is lower than the front edge of CME-1 indicating that CME-2 would arrive at the Earth later than CME-1. Thus, CME-2 was the solar source of the ICME-2. It should be noted that, based on the fitting

results of GCS model, CME-2 is faster than CME-1 and their propagation directions are close to each other. Thus, these two CMEs are expected to interact in interplanetary space. Seen from the in situ observations, possible interaction region signatures were detected between these two ICMEs with lower magnetic field, higher velocity, high density, and higher plasma beta. Furthermore, similar analysis shows that CME-3 might arrive at Earth after September 7 19:21 UT. Considering the long duration of Ejecta-4 and the larger angular width of CME-3, we verify that CME-3 is the solar source of ICME-4 and the driver of the second shock. It should be noted that, no obvious Earth-directed CME could be identified as the solar source of Ejecta-3. A possible explanation is that this ejecta structure is formed in the sheath region of ICME-4 during its propagation outward (e.g., Zheng & Hu 2018, and reference therein).

## 3. The Importance of Shock-ICME Complex Structure in Causing the Geomagnetic Storm

Based on the observational analysis in Section 2, we find that the intense geomagnetic storm with the peak value of −142 nT is caused by the shock-ICME structure. Seen from Panel (b) in Figure 1, the $B_s$, which is equal to the negative value of $B_z$, jumps from ∼10 nT to ∼30 nT at the shock inside ICME2. As the $B_s$ or the dawn–dusk electric field ($v_x B_s$) is a main factor in determining the intensity of a geomagnetic storm (e.g., Gonzalez et al. 1994), we can expect that such enhancement of $B_s$ do significantly enhance the intensity of this geomagnetic storm. But, the question is: by how much does the shock enhance the geoeffectiveness of this ICME?

Recently, Wang et al. (2018) developed a method to recover the shocked part of the magnetic cloud to the uncompressed state. One can refer to Section 3.2 of their paper for details. For the completeness of the paper, we repeatedly describe the method below. This method simply assumes that: (1) the magnetic field, plasma velocity, and density in the sheath region can be related to the uncompressed state by the shock relation, i.e., Rankine–Hugoniot (R–H) jump conditions, and (2) the shock normal ($\hat{n}$), shock speed ($v_s$), and the compression ratio ($r_c$), are the same as those at the observed shock surface. Treating the sheath region as the downstream (using subscript "2") of the shock, the uncompressed state, i.e., the parameters of the upstream (using subscript "1") of the shock, can be given by the following equations:

$$\rho_1 = \frac{1}{r_c}\rho_2 \tag{1}$$

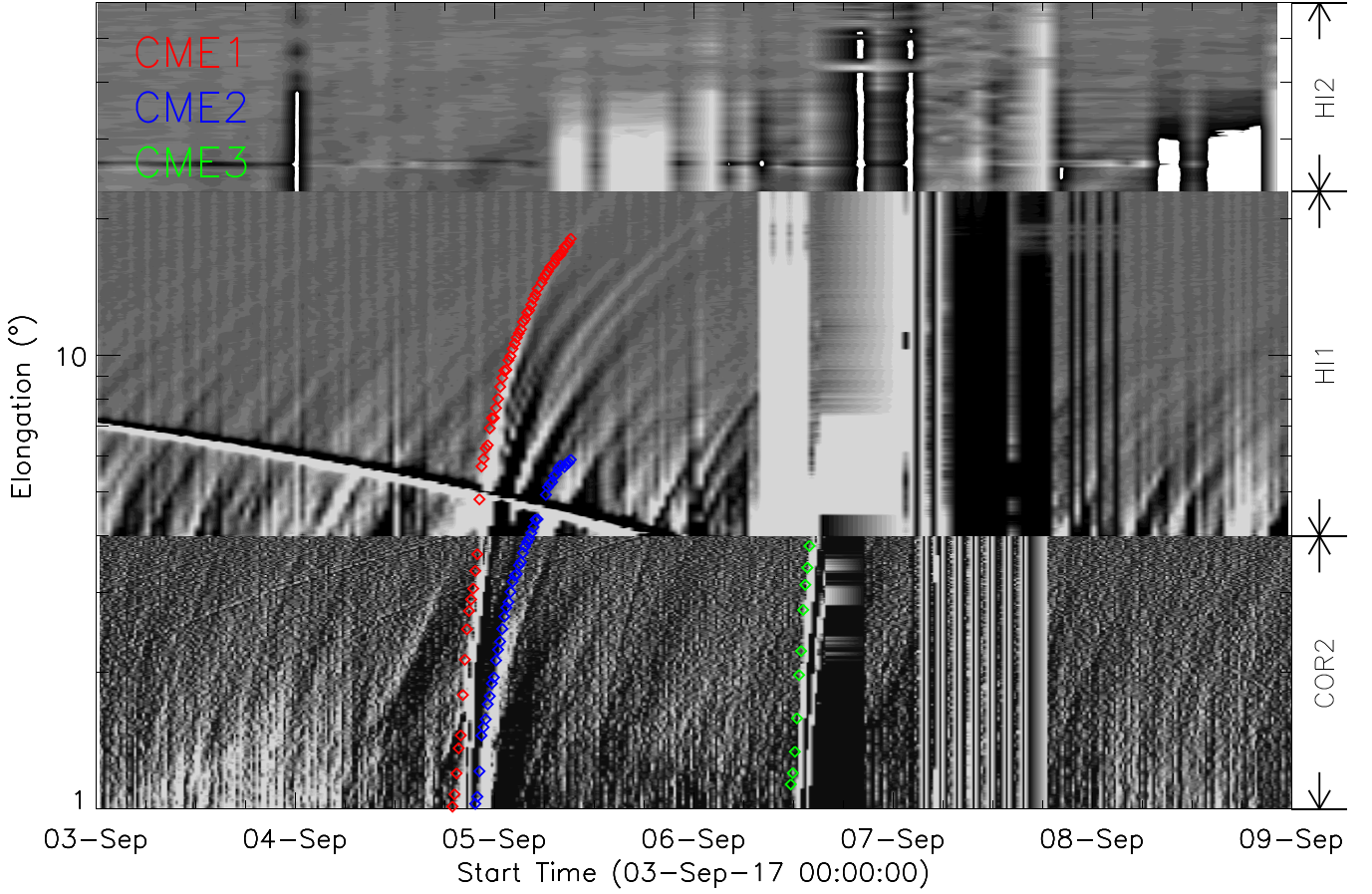$$\boldsymbol{B}_{1n} = \boldsymbol{B}_{2n} \tag{2}$$

**Figure 3.** Time-elongation angle map from 2007 September 4 to 9 based on *STEREO A* observations. Different colors show the measurements of the front edges of different CMEs.

$$B_{1\perp} = \frac{v_{A2}^2 - u_2^2}{v_{A2}^2 - r_2 u_2^2} B_{2\perp} \qquad (3)$$

$$u_{1n} = r_c u_{2n} \qquad (4)$$

$$u_{1\perp} = \frac{v_{A2}^2 - u_2^2}{v_{A2}^2 - r_2 u_2^2} r_c u_{2\perp} \qquad (5)$$

in which $\rho$ is the density including the protons and electrons, $B$ represents the magnetic field, $u$ is the solar wind speed in the DeHoffman–Teller (HT) frame, and $v_A$ is the Alfvén speed. The subscript "$n$" and "$\perp$" mean the component parallel and perpendicular to the shock normal. The recovered interval is longer than the observed shocked interval, and its duration is calculated based on the mass conservation with the formula of $dt_1 = \frac{u_{2n} + vs}{u_{1n} + vs} r_c dt_2$. The shock parameters can be obtained based on the R–H analysis (e.g., Koval & Szabo 2008, and references therein). In this case, the parameters of shock inside ICME2 are: shock normal ($\hat{n}$) direction in GSM coordinate = [−0.83, 0.3, −0.46], shock speed $v_s = 759$ km s$^{-1}$, and compression ratio $r_c = 2.23$.

Figure 6 shows the *Wind* observations of the magnetic field and solar wind velocity vectors (black lines) and the recovered uncompressed state of these parameters (red lines) of the Shock-ICME complex structure (ICME-2). The shaded region shows the observed shock-ICME region. The black lines between the first two vertical lines show the original observations, and the red lines between the first and third

vertical lines represent the recovered parameters. Seen from this figure, the intensity of the magnetic field and the solar wind velocity would become much smaller if there was no shock compression. Using the recovered state of the ICME, we can then quantitatively estimate the enhancement of ICME's geoeffectiveness. Previous studies show that the peak value of the Dst index is well correlated with the value of the $B_s$ and the dawn–dusk electric field ($v_x B_s$; e.g., Wang et al. 2003b; Wu & Lepping 2016; Shen et al. 2017a, and references therein). Based on the in situ observation, the peak values of $B_s$ and $v_x B_s$ in this ICME were 31 nT and −13 mv m$^{-1}$, respectively. But, if the shock compression did not happen, the peak values of $B_s$ and $v_x B_s$ would decrease to 13 nT and −6.4 mv m$^{-1}$, according to the recovered uncompressed results. Shen et al. (2017a) have shown a statistical correlation between the $v_x B_{s,\text{min}}$ and Dst$_{\text{min}}$. It is Dst$_{\text{min}} = 8.48(v_x B_s)_{\text{min}}$ (mv m$^{-1}$)−24.5. Based on this correlation, we can estimate that the value of Dst$_{\text{min}}$ is −135 nT by using observed $v_x B_s$ or −79 nT by using the recovered $v_x B_s$. It can be seen that the calculated value of the Dst$_{\text{min}}$ from the observational solar wind data is similar with the real observed value (−142 nT). Besides, without the shock compression, the peak value of the Dst index would decrease greatly. The possible peak value is −79 nT, which is larger than −100 nT. Thus, there would only be a moderate geomagnetic storm if the ICME was not compressed by the shock. Using the peak Dst index as a measure, we can calculate that the shock compression enhanced the intensity of the geomagnetic storm by a factor of two (∼1.8). In addition, other Dst index forecasting models are applied to the observed and recovered
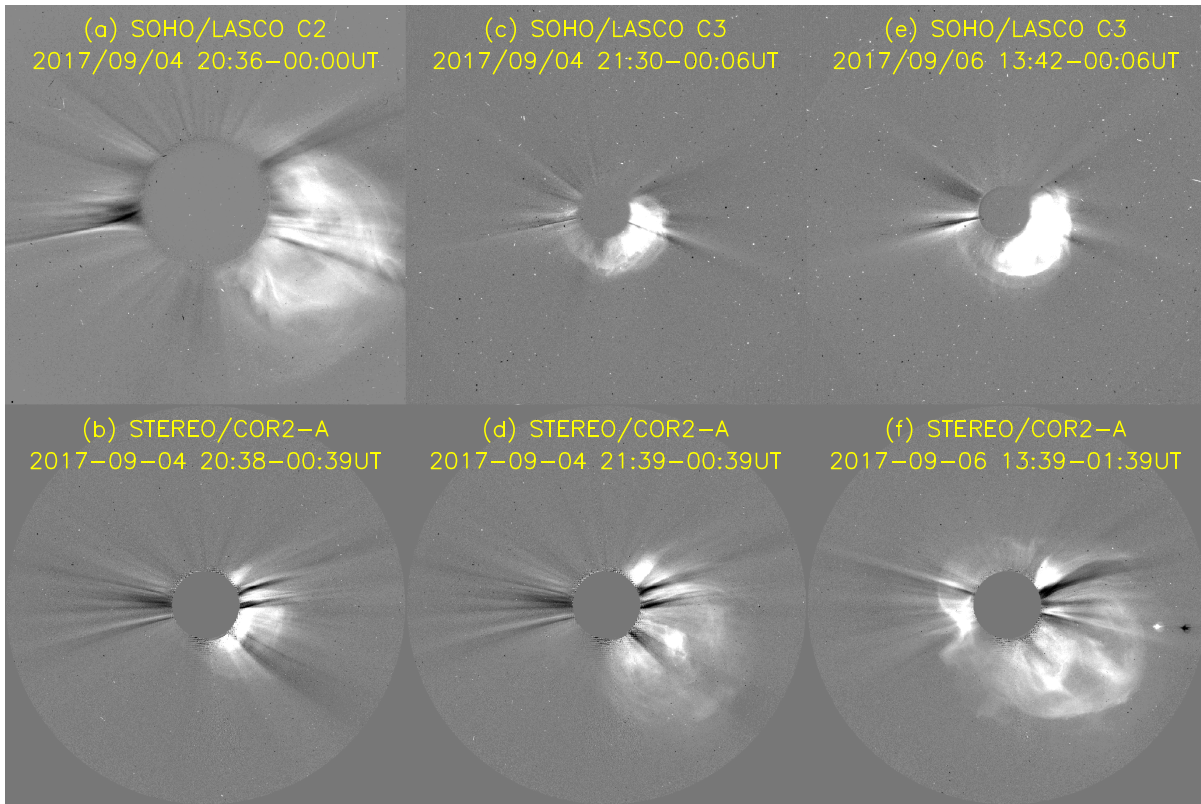
**Figure 4.** *SOHO*/LASCO and *STEREO*/*SECCHI* observations the 2017 September 4 19:48 UT (panel (a) and (c)), 2017 September 4 20:36 UT (panel (b) and (e)) and 2017 September 6 12:24 UT (panel (c) and (f)) CMEs.
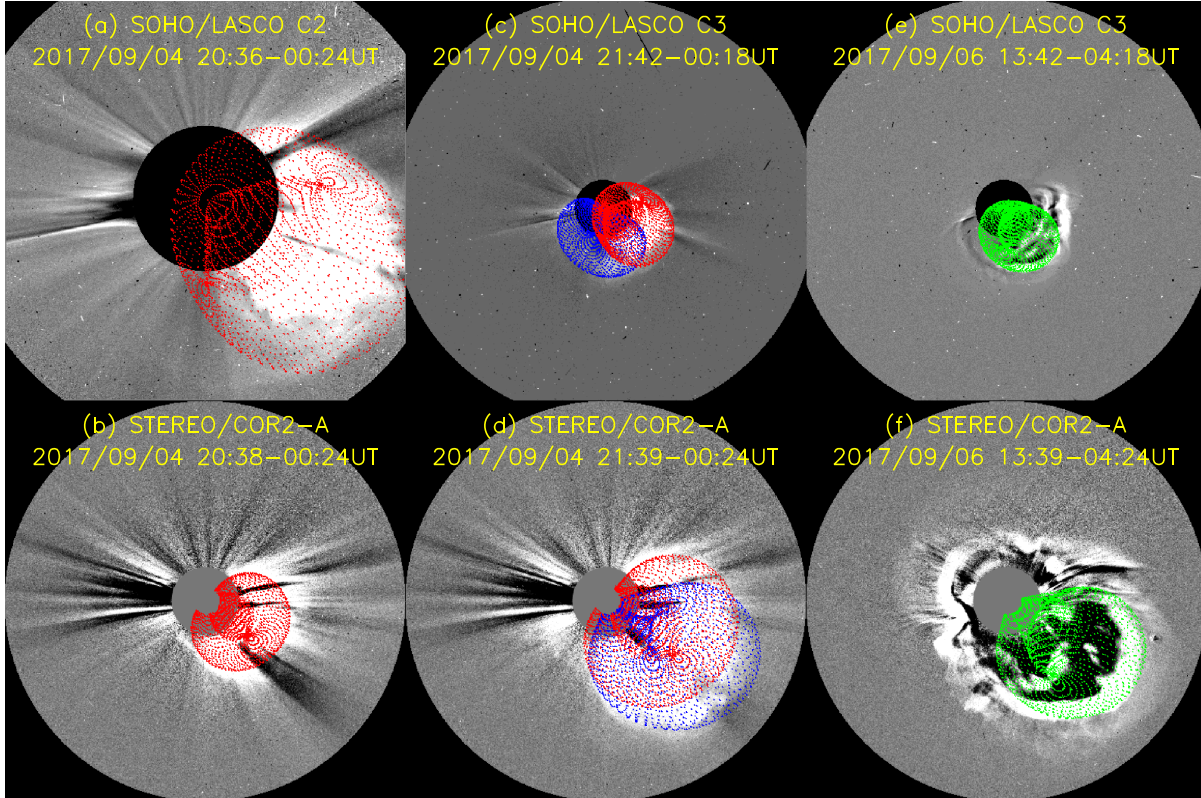


**Figure 5.** The coronagraph images of these CMEs with GCS wireframe overlaid on top. Red, blue, and green colors show the fitting results for CME-1, CME-2, and CME-3, respectively.
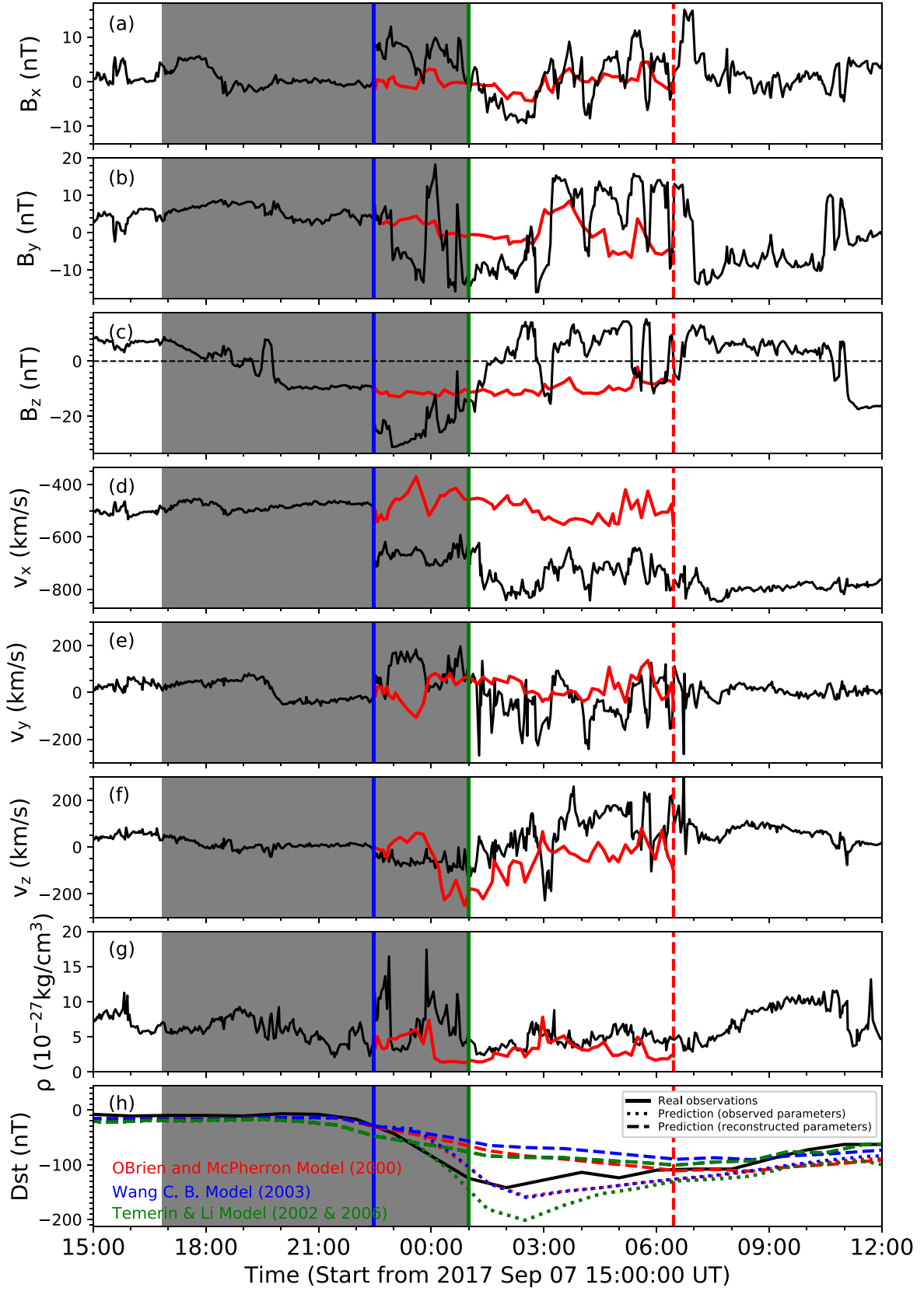
**Figure 6.** The observational data and recovered uncompressed state of magnetic field, solar wind speed, total plasma density, and Dst index from 2017 September 6 12:00 to 2017 September 8. The shaded region shows the period of the ICME and the blue line shows the time of the shock arrival. The black lines in panels (a) to (h) between the first two vertical lines (blue and green vertical lines) show the original observations, and the red lines between the first and third vertical lines (blue and red vertical lines) represent the recovered parameters. Panel (h) shows the real data (black line) and the prediction results based on the observed (dashed lines) and recovered (dashed–dotted lines) parameters of the Dst index. Different colors represent different prediction methods.
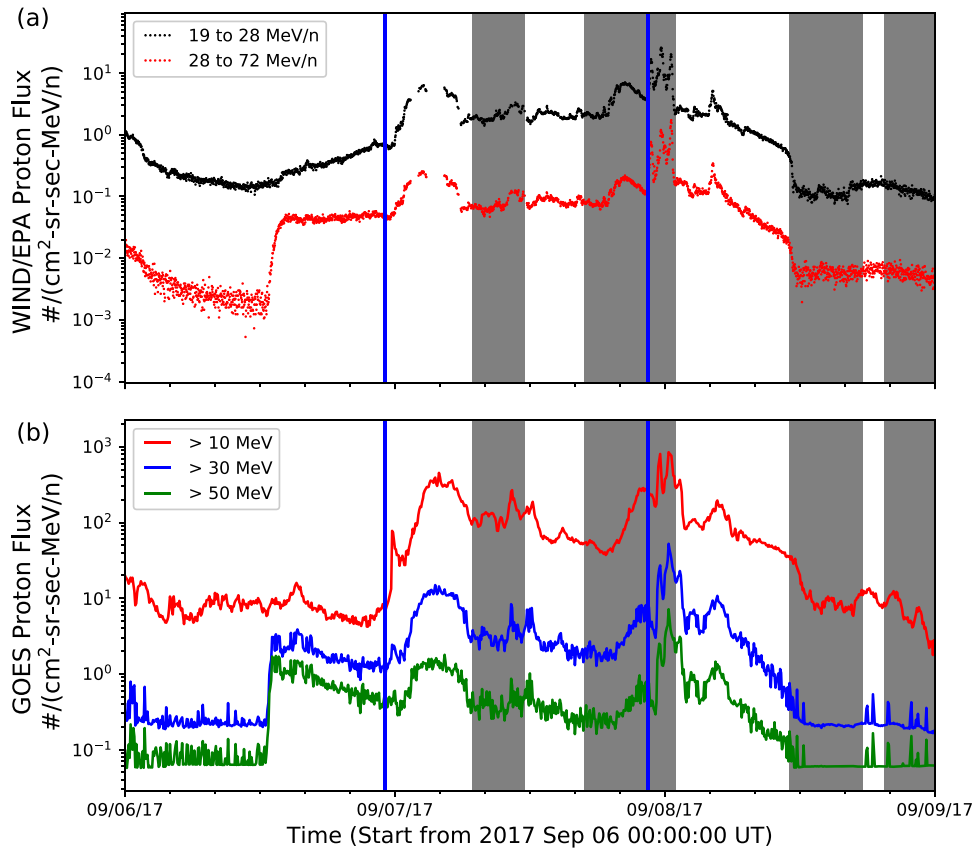
**Figure 7.** The observations of the flux of high-energy protons from *Wind*/EPA (panel (a)) and *GOES* (panel (b)) during the period from 2017 September 6 to 8. Different colors represent different energy channels. The four shaded regions show four ICMEs and two blue vertical lines show the shock positions.

solar wind parameters. Panel (h) in Figure 6 shows the result. The black line shows the real observation of the Dst index. The dashed lines and dashed–dotted lines show the magnetosphere prediction results based on the observed and recovered parameters, respectively. Red, blue, and green lines show the results from OBrien and McPherron (OM) model (O'Brien & McPherron 2000), Wang model (Wang et al. 2003a), and Temerin and Li (TL) model (Temerin & Li 2002), respectively. Seen from this panel, all of these models can well predict the tendency of the Dst variation by using the real solar wind parameters. But, the predicted peak values of Dst are all higher than real observations. They are −158 nT (OM model), −160 nT (Wang model), and −202 nT (TL model). Meanwhile, by using the recovered parameters, the predicted Dst index decreases much slower and the predicted peak values of Dst index are −112, −91, and −101 nT for the respective models. Compared with prediction results using the real solar wind observations, ratios between the peak values of Dst are of 1.4, 1.8, and 2 for different models, respectively. Thus, combined with these results, we suggest that the shock compression enhanced the geoeffectiveness of ICME-2 by an average of 1.73. Without shock compression, ICME-2 would only cause a moderate geomagnetic storm.

## 4. The Proton Flux Signature in the Shock-ICME Structure

The proton flux enhancement during a shock-MC structure in 2011 November 5 event has been reported by Shen et al. (2008). In the present study, the characteristics of high energetic proton flux are also provided. Figure 7 shows the high-energy proton observation from *Wind*/EPA (panel (a))

and *GOES* (panel (b)). Different colors represent different energy channels. Seen from these panels, the proton flux decreased at the front edges of the shaded regions 1 and 3. Meanwhile, it increased at the trailing edges of these regions. This indicates that the proton flux intensities in the Ejecta-1 and the Ejecta-3 are lower than those in background. This is consistent with the normal situation (e.g., Cane & Lario 2006, and references therein). However, for the shaded region 2, which is the shock-ICME complex structure, the proton flux intensities increased at its front edge and decreased at its trailing edge for almost all energy channels. At the front edge, the intensity of energy ⩾10 MeV protons jumped by about five times, from ∼40 pfu to ∼200 pfu. In addition, the arrival of the shock further enhanced this intensity. At the trailing edge of this region, the proton flux intensity decreased about 10 times from ∼800 pfu to ∼80 pfu. This means that the proton flux intensity in this structure was obviously higher than that in the background. In addition to the 2001 November event reported by Shen et al. (2008), this is another definitive case that shows the shock-ICME complex structure leads to a significantly enhancement in the proton flux intensity.

## 5. Conclusion and Discussion

In this work, we studied the interplanetary signature and the cause of the intense geomagnetic storm in the early days of 2017 September in detail. Based on the in situ observations, we found that there were three obvious ICMEs and one ICME-like structure. Two ICMEs drove shocks ahead of them. It is noteworthy that the shock driven by following structure propagated into ICME-2 and then formed a shock-ICME

complex structure. The space weather effect of these ICMEs, especially the shock-ICME complex structure, was further discussed. The main findings of this work are as follows:

1. These ICMEs caused a multiple step intense geomagnetic storm with the peak value of the Dst index of −142 nT. The shock-ICME complex structure formed by ICME-2 and shock driven by ICME-3 was the main interplanetary cause of this intense geomagnetic storm.

2. Using the recovering method developed by Wang et al. (2018), we showed that the shock compression in ICME-2 obviously enhanced the magnetic field and also the geoeffectiveness of this ICME. A quantitative analysis showed that this ICME would only cause a moderate geomagnetic storm if no compression happened. The compression of the magnetic field by the shock enhanced the intensity of this geomagnetic storm by roughly a factor of two.

3. The high-energy proton flux in this shock-ICME complex structure was obviously enhanced, which was similar to another shock-ICME event reported by Shen et al. (2008). The proton flux intensity in the shock-ICME complex structure was about five times higher than that in the background, which make this SEP event stronger.

In this work, we showed the enhancement of the ICMEs' geoeffectiveness caused by the shock compression quantitatively based on the observations for the first time. Our results showed that the ICME-2 would only cause a moderate geomagnetic storm without the compression of the ICME by the shock. Meanwhile, we also found that the proton flux intensity was enhanced in this shock-ICME complex structure. These findings further strength the viewpoint that the multiple CMEs interaction, especially the shock-ICME interaction, is an important factor in the space weather effect of CMEs. However, questions still remain. The first question is: how do we forecast the shock-ICME interaction based on the solar observations of CMEs? The second question is: which parameters would influence the geoeffectiveness and SEP intensity enhancement? Especially, we reported two proton flux enhancements events due to the shock-ICME complex structures. Does this occur in all shock-ICME complex structures? To answer these questions, more detailed and statistical analyses should be pursued.

## References

Burlaga, L. F., Plunkett, S. P., St, & Cyr, O. C. 2002, JGR, 107, 1266
Cane, H. V., & Lario, D. 2006, SSRv, 123, 45
Colaninno, R. C., & Vourlidas, A. 2015, ApJ, 815, 70
Gonzalez, W. D., Joselyn, J. A., Kamide, Y., et al. 1994, JGR, 99, 5771
Gopalswamy, N., Lara, A., Manoharan, P., & Howard, R. 2005, AdSpR, 36, 2289
Gopalswamy, N., Lara, A., Yashiro, S., Kaiser, M. L., & Howard, R. A. 2001a, JGR, 106, 29207
Gopalswamy, N., Yashiro, S., Kaiser, M. L., Howard, R. A., & Bougeret, J. L. 2001b, ApJL, 548, L91
Ivanov, K. G. 1982, SSRv, 32, 49
Kaiser, M. L., Kucera, T. A., Davila, J. M., et al. 2008, SSRv, 136, 5
Koval, A., & Szabo, A. 2008, JGR, 113, A10110
Lepping, R. P., Burlaga, L. F., Szabo, A., et al. 1997, JGR, 102, 14049
Lugaz, N., Farrugia, C. J., Davies, J. A., et al. 2012, ApJ, 759, 68
Lugaz, N., Farrugia, C. J., Huang, C. L., & Spence, H. E. 2015a, GeoRL, 42, 4694
Lugaz, N., Farrugia, C. J., Smith, C. W., & Paulson, K. 2015b, JGRA, 120, 2409
Lugaz, N., Kintner, P., Möstl, C., et al. 2012, SoPh, 279, 497
Lugaz, N., Manchester, W. B. I. V., & Gombosi, T. I. 2005, ApJ, 634, 651
Lugaz, N., Temmer, M., Wang, Y., & Farrugia, C. J. 2017, SoPh, 292, 64
Manchester, W., Kilpua, E. K., Liu, Y. D., et al. 2017, SSRv, 212, 1159
Mishra, W., Wang, Y., Srivastava, N., & Shen, C. 2017, ApJS, 232, 5
O'Brien, T., & McPherron, R. L. 2000, JASTP, 62, 1295
Shen, C., Chi, Y., Wang, Y., Xu, M., & Wang, S. 2017a, JGRA, 122, 5931
Shen, C., Wang, Y., Pan, Z., et al. 2014, JGRA, 119, 5107
Shen, C., Wang, Y., Wang, S., et al. 2012a, NatPh, 8, 923
Shen, C., Wang, Y., Ye, P., & Wang, S. 2008, SoPh, 252, 409
Shen, F., Feng, X. S., Wang, Y., et al. 2011, JGR, 116, A09103
Shen, F., Wang, Y., Shen, C., & Feng, X. 2017b, SoPh, 292, 104
Shen, F., Wu, S. T., Feng, X., & Wu, C. C. 2012b, JGRA, 117, 1
Temerin, M., & Li, X. 2002, JGRA, 107, 1472
Temmer, M., Rollett, T., Möstl, C., et al. 2011, ApJ, 743, 101
Temmer, M., Veronig, A. M., Peinhart, V., & Vršnak, B. 2014, ApJ, 785, 85
Temmer, M., Vršnak, B., Rollett, T., et al. 2012, ApJ, 749, 57
Thernisien, A. 2011, ApJS, 194, 33
Thernisien, A., Vourlidas, A., & Howard, R. A. 2009, SoPh, 256, 111
Thernisien, A. F. R., Howard, R. A., & Vourlidas, A. 2006, ApJ, 652, 763
Vandas, M., Fischer, S., Dryer, M., et al. 1997, JGR, 102, 22295
Vršnak, B. 2001, SoPh, 202, 173
Vršnak, B., & Žic, T. 2007, A&A, 472, 937
Wang, C. B., Chao, J. K., & Lin, C. H. 2003a, JGRA, 108, 1341
Wang, Y., Shen, C., Liu, R., et al. 2018, JGRA, in press (doi:10.1002/2017JA024971)
Wang, Y., Shen, C. L., Wang, S., & Ye, P. Z. 2003b, GeoRL, 30, 2039
Wang, Y. M., Ye, P. Z., & Wang, S. 2003c, JGRA, 108, 1370
Wang, Y. M., Ye, P. Z., Wang, S., & Xiong, M. 2003d, SoPh, 216, 295
Wang, Y. M., Ye, P. Z., Wang, S., & Xue, X. H. 2003e, GeoRL, 30, 31
Wu, C. C., & Lepping, R. P. 2016, SoPh, 291, 265
Xiong, M., Zheng, H., Wang, Y., Wang, S., & Wu, S. T. 2006, JGR, 111, 11102
Yan, X. L., Wang, J. C., Pan, G. M., et al. 2018a, arXiv:1801.02290
Yan, X. L., Yang, L. H., Xue, Z. K., et al. 2018b, arXiv:801.02738v1
Zheng, J., & Hu, Q. 2018, ApJL, 852, L23